JOURNAL OF GEOPHYSICAL RESEARCH, VOL. 93, NO. B9, PAGES 10,408–10,420, SEPTEMBER 10, 1988

Global Distribution of Seamounts from Seasat Profiles

CLAIRE H. CRAIG[1] AND DAVID T. SANDWELL

Center for Space Research, University of Texas at Austin

Bathymetric profiles and contour charts have been used to study the distribution of seamounts in the deep ocean basins, but only a small fraction of the seafloor has been sampled by ships. At the present exploration rate it will take several centuries to map significant portions of the seafloor topography. Satellite altimetry, which maps the topography of the equipotential sea surface, is a promising tool for studying the gravity fields of seamounts because all ocean basins can be sampled in a couple of years. Using a model of a Gaussian-shaped seamount loading a thin elastic lithosphere, we develop a new technique for measuring basic characteristics of a seamount from a single satellite altimeter profile. The model predicts that the seamount diameter is equal to the peak-to-trough distance along the vertical deflection profile and that the overall diameter of the signature reveals the age of the lithosphere when the seamount formed. Moreover, the model suggests that these two measurements are relatively insensitive to the cross-track location of the seamount. We confirm these model predictions using Seasat altimeter profiles crossing 14 well surveyed seamounts in the Pacific. We then apply the measurement technique to 26 x 10^6 million kilometers of Seasat profiles resulting in a new global set of seamount locations. Approximately one quarter of the seamounts identified in Seasat profiles were previously uncharted. Modeling suggests that there is no direct relationship between the size of a seamount and its signature in the geoid; therefore the set of locations is not a straightforward sampling of the total seamount population, but is weighted toward seamounts which are poorly compensated. A preliminary analysis indicates considerable variations in population density and type across the oceans; most notable among them are the absence of seamounts in the Atlantic, variations in population density across large age-offset fracture zones in the Pacific, the prevalence of small signatures in the Indian Ocean, and the existence of linear trends in the large seamounts of the west Pacific.

INTRODUCTION

Oceanic intraplate topography mainly consists of volcanic islands and seamounts. A seamount is an isolated elevation on the seafloor with a circular or elliptical shape, at least 1 km high, with comparatively steep slopes and relatively small summit area [*Menard*, 1964]. This morphology, along with their mostly basaltic composition, reveals the volcanic origin of seamounts. Several factors may control the birth and development of seamounts (undersea volcanoes). First, there must be an adequate supply of heat or magma beneath the lithosphere. Second, the magma must have enough hydraulic head [*Vogt*, 1974] and latent heat to penetrate the strong oceanic lithosphere without freezing during ascent [*Spence and Turcotte*, 1985]. Finally, the lithosphere must remain over the heat source or magma pool long enough for the volcano to develop [*Gass et al.*, 1978]. Existing observations of seamount distribution and seamount formation age do not yet discriminate among these three factors.

Most seamounts in the world's oceans are uncharted because only a small fraction of the seafloor has been mapped by ships. Moreover, the distribution of ship data is very irregular, and the coverage of the southern oceans is particularly poor. Even among seamounts that have been detected, little is known about their morphologies and formation histories. Despite the sampling problems, previous attempts have been made characterize the spatial and size distributions of seamounts. Map counts of the number of seamounts on a given age of seafloor indicate that the production rate of small undersea volcanoes decreases as the lithosphere ages [*Batiza*, 1981]. More recent compilations of seamount data, using individual bathymetric profiles rather than highly interpolated contour maps, show that earlier estimates of seamount population density are an order of magnitude too small [*Jordan et al.*, 1983; *Smith and Jordan*, 1988]. Ninety percent of undersea volcanoes with height less than 1 km are uncharted because they lie between available bathymetric profiles. Moreover, it is predicted that half of the seamounts taller than 1 km are uncharted; most of these seamounts lie in the remote southern ocean basins.

These more detailed analyses indicate that small seamounts are much more abundant than large ones and that the size-frequency distribution is Poissonian; the number of seamounts with height above a given value falls off exponentially with increasing height [*Jordan et al.*, 1983; *Smith and Jordan*, 1988]. Their results also suggest that production rates depend not only on the age of the lithosphere but also on the extent of the magma source. However, these findings are based on only 157,000 km of bathymetric profiles. To sample completely the oceans with a 10-km spacing will take at least 1000 times more data. It is unlikely that this much data will ever be collected by ships.

Satellite altimetry, which maps the topography of the equipotential sea surface, is a promising tool for studying the distribution of seamounts because all ocean basins can be sampled in a couple of years. While the coverage by the Seasat altimeter is relatively uniform between latitudes of 72°N and 60°S, it is still incomplete because Seasat failed prematurely. The largest gaps in the Seasat data are diamond-shaped areas with dimensions of about 100 km. Because the typical spacing of altimeter profiles is greater than the typical diameter of a seamount, the altimeter data cannot be interpolated and gridded prior to seamount studies; the original profiles must be used. In the first part of the paper we develop a technique for measuring three basic characteristics of a seamount using a single satellite altimeter profile. They are the along-track location of a seamount, the characteristic diameter of a seamount, and the age of the lithosphere when the seamount formed.

Seamounts are apparent in GEOS-3 and Seasat altimeter profiles because they produce small bumps in the sea surface or geoid

[1]Now at Home Office, London.

Paper number 7B2027.
01488-0227/88/007B-2027$05.00

[*Lambeck and Coleman,* 1982; *Lazarewicz and Schwank,* 1982; *Sandwell,* 1984*a, b*]. With Seasat data, the along-track position of a seamount can be determined to an accuracy of 10 km or less. However, its cross-track position cannot be determined unless the seamount is intersected by more than one profile [*Baudry et al.,* 1987]. Features as small as 20 km in diameter can be resolved using Seasat data. This positioning accuracy and resolution is 10–100 times worse than that of deepwater bathymetric profilers. Nonetheless, many previously uncharted seamounts have been discovered by comparing altimeter profiles to bathymetric charts. In several cases these newly discovered seamounts have been confirmed by shipboard surveys [*Baudry and Diament,* 1988].

In addition to locating seamounts it has been shown that the strength of the lithosphere (which depends mainly on age), at the time of volcanic loading, can be inferred from satellite altimeter data if good bathymetric data are also available [*Watts and Ribe,* 1984]. However, only a few seamounts are surveyed well enough to perform this analysis, and most of these lie in the northern oceans. To analyze unsurveyed seamounts, or seamounts with poor bathymetric coverage, we have developed a new measurement technique based on a model of a Gaussian seamount loading a thin elastic lithosphere. The model predicts that the seamount diameter is equal to the peak-to-trough distance along the vertical deflection profile (i.e., the along-track slope of the geoid) and that the overall diameter of the signature reveals the age of the lithosphere when the seamount formed. Moreover, the model suggests that these two measurements are relatively insensitive to the cross-track location of the seamount, although the accuracies of these measurements are dependent on the amplitude of the geoid signature. We confirm these model predictions using Seasat altimeter profiles crossing 14 well surveyed seamounts in the Pacific.

After developing and testing the measurement technique we use 26 x 10^6 km of Seasat profiles to locate and measure large seamounts in the world's oceans. The uniform sampling enables us to compare seamount population densities on a global basis. To enhance the short-wavelength signatures of seamounts, each geoid profile is differentiated, resulting in along-track deflections of the vertical [*Sandwell,* 1984*a, b*]. Seamounts are located through a visual examination of the data. The amplitude and width of each seamount signature are then measured by computer. Several important characteristics of seamount populations are derived from these measurements: the global population density, its size-frequency distribution, and the amplitude-frequency distribution of the gravitational signals.

SEAMOUNT MODEL

The model consists of a Gaussian-shaped seamount loading a thin elastic lithosphere (Figure 1). The form of the seamount load is

$$h(r) = A \exp\left[\frac{-r^2}{2\sigma^2}\right] \quad (1)$$

where A is the height of the seamount and σ is the characteristic radius at an elevation of $0.6A$. The plate flexes under the load, causing a depression in the seafloor and Moho. Assuming that the flexural response is linear and the height of the seamount is small compared with the water depth, the geoid height N at a distance r from the center of the seamount is

$$N(r) = \frac{1}{2\pi}\int_0^\infty Q(k)\ H(k)\ J_0(kr)\ k\ dk \quad (2)$$

where $H(k)$ is the Hankel transform of $h(r)$ [*Bracewell,* 1978, p. 248],

$$H(k) = 2\pi\sigma^2 A \exp\left[-\frac{\sigma^2 k^2}{2}\right] \quad (3)$$

and $Q(k)$ is the geoid/topography transfer function for surface loading of a thin elastic plate. The transfer function usually relates the topography to the geoid. However, in this model the Gaussian-shaped seamount is used as a load which produces additional flexural topography. The transfer function includes an additional term to account for the topography due to flexure. It was derived following the technique of *Banks et al.* [1977]. It is

$$Q(k) = \frac{2\pi G(\rho_c-\rho_w)}{gk} e^{-ks}\left[1 - R_c(k)e^{-kd}\right]\left[1 - \frac{(\rho_c-\rho_w)}{(\rho_m-\rho_w)} R_w(k)\right] \quad (4)$$

where

$$R_c(k) = \left[1 + \frac{D k^4}{g(\rho_m - \rho_c)}\right]^{-1} \quad (5)$$

and

$$R_w(k) = \left[1 + \frac{D k^4}{g(\rho_m - \rho_w)}\right]^{-1} \quad (6)$$

where G is the gravitational constant, g is the acceleration of gravity, ρ_w (1025 kg/m^3) is the seawater density, ρ_c (2800 kg/m^3) is the crustal density, and ρ_m (3330 kg/m^3) is the mantle density.

The flexural rigidity of the plate, D, increases with increasing lithospheric age t. Assuming that the thermal boundary layer cooling model applies at ages less than 70 Ma, the flexural rigidity is [*Sandwell and Schubert,* 1982]

$$D = \frac{2E(kt)^{3/2}}{3(1 - \nu^2)}\left\{erfc^{-1}\left[\frac{T_m - T_e}{T_m - T_o}\right]\right\}^3 \quad (7)$$

where E (6.5 x 10^{10} Pa) is Young's modulus, ν (0.25) is Poisson's ratio, T_o (0.0°C) is the surface temperature, T_e (450°C) is the temperature at the base of the elastic layer and T_m (1365°C) is the mantle temperature. The flexural rigidity increases as the age to the 3/2 power.

Equation (2) was numerically integrated to determine the geoid height versus the distance r from the center of the seamount. Because the Earth's geoid is dominated by long-wavelength components, seamount signatures are most apparent after satellite altimeter profiles are differentiated along-track [*Sandwell,* 1984*a, b*]. Model along-track vertical deflection profiles were calculated by differentiating model geoid profiles whose closest approach was a distance of y_c (Figure 1) from the center of the seamount. The important model parameters are the height A and radius σ of the seamount, the age of the lithosphere when the seamount formed t, and the minimum distance between the center of the seamount and the satellite profile, y_c.

Modeling results confirm the findings of *Watts and Ribe* [1984] that the amplitude of the vertical deflection signature is not a good measure of the height of the seamount. This is because the amplitude also depends upon the age of the lithosphere when the seamount formed, as shown in Figure 2. The three vertical deflection profiles were calculated for a seamount with a height of 2 km and a characteristic radius of 10 km. As the seamount is placed on older and more rigid lithosphere, the vertical deflection signature increases in amplitude and in width. The most important finding is that the distance between the peak and trough of the vertical deflection profile is about equal to the diameter (2σ) of the seamount. Moreover, this distance is largely independent of the strength (loading age) of the lithosphere. Since the amplitude of the vertical deflection signature is linearly related to the seamount height, the peak-to-trough distance is also independent of seamount height.

Another important finding is that overall diameter of the expres-

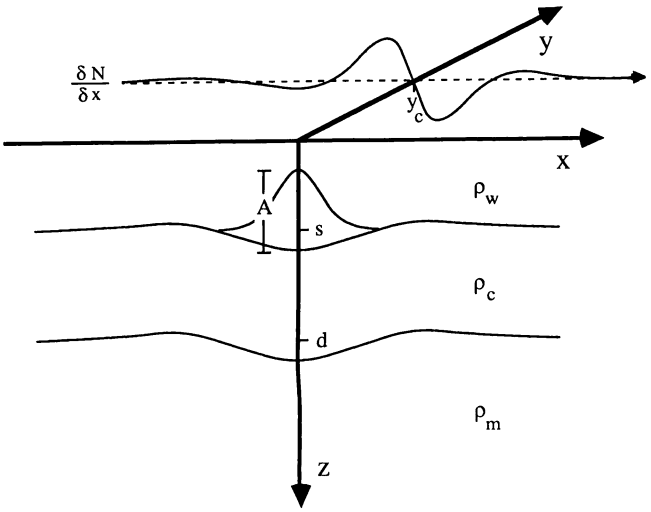

Fig. 1. Model of Gaussian-shaped seamount with radial symmetry loading a thin elastic lithosphere. The satellite altimeter profile passes over the seamount at a distance y_c from its center.The along-track vertical deflection profile has a characteristic peak-and-trough signature associated with the bump in the geoid.

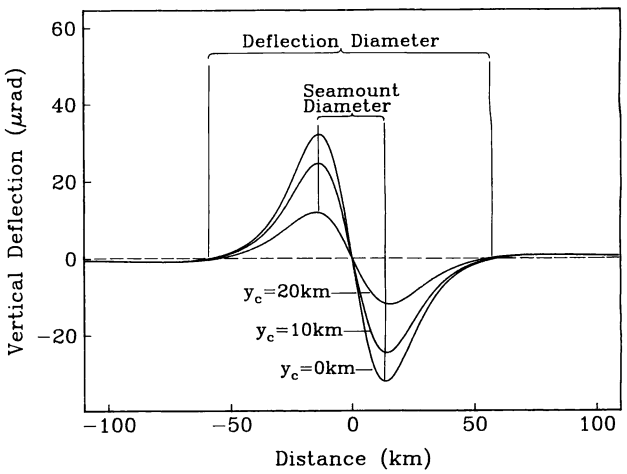

Fig. 3. Vertical deflection profiles that pass at three distances from the center of the seamount, y_c. The peak-to-trough distance is a good measure of the seamount's diameter and is independent of y_c. The deflection diameter (zero crossing to zero crossing) is related to the loading age and is also independent of y_c.

sion (zero crossing to zero crossing) depends mainly lithospheric strength (Figure 2) and therefore could be used to determine the age of the lithosphere when the seamount formed. The model predicts that the overall diameter minus the seamount diameter is equal to the flexural diameter, which depends only on the loading age. The flexural diameter increases monotonically with age from 64 km at 4 Ma to 160 km at 73 Ma. In practice, it is very difficult to measure these zero crossings because the gradient of the signature is low. In future studies we hope to overcome this measurement problem by fitting an empirical model to observed vertical deflection signatures and extrapolating the model to determine the zero crossings.

A possible problem in measuring the diameter of a seamount using this method is that it is not known whether the profile passes directly over the center of the seamount unless, of course, good bathymetric data are available. To determine the error associated with this measurement, we calculated model profiles using three different values of y_c (Figure 3). The amplitude of the vertical deflection signature decreases as y_c is increased, but neither the peak-to-trough distance (seamount diameter) nor the zero-crossing diameter (deflection diameter) depends strongly on y_c. However, as the profile is moved away from the seamount, it becomes increasingly more difficult to measure these diameters. When the profile misses the the seamount entirely, its signature is too small to be detected in the presence of noise. The results from this simple model imply that the radius of a seamount can be measured from a single satellite altimeter profile that intersects any part of the seamount.

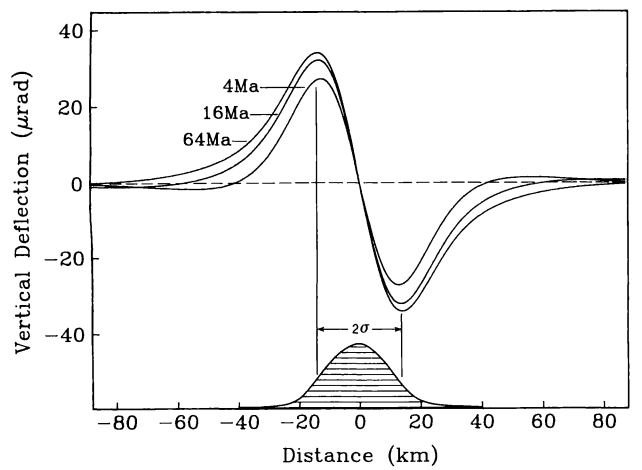

Fig. 2. Vertical deflection profiles for a Gaussian-shaped seamount (A = 2 km, σ = 10 km) loading the lithosphere at three different ages. The signature increases in amplitude and broadens as the loading age increases.

TESTING THE MODEL PREDICTIONS

Seasat altimeter measurements of the sea surface topography (geoid) were edited to remove bad data points and were high-pass filtered by subtracting a geoid calculated from the spherical harmonic coefficients of the PGS-S4 gravity model to degree and order 26 [*Marsh and Martin*, 1982]. The deflection of the vertical was calculated from the geoid and then plotted along ascending and descending satellite ground tracks separately on the General Bathymetric Chart of the Oceans (GEBCO) 1:10^7 maps [*Canadian Hydrographic Service*, 1982]. Each data point represents the average of 1000 radar pulses. The points are spaced at 6.6-km intervals along the track. The resolution of the data is limited by the altimeter noise that dominates the signal at wavelengths less than about 30 km.

Fourteen well surveyed seamounts, from various parts of the Pacific basin, were used to test the model predictions. Sixty-three seamounts were chosen initially, but only 14 were intersected by at least one Seasat profile. This suggests that less than 25% of the seamount population is sampled by Seasat profiles. About half of the seamount data were collected during multibeam sonar surveys [*Smoot*, 1981, 1982, 1983; *Vogt and Smoot*, 1984]. The remaining published seamount data are from single-beam sonar profiles [*Sager*, 1983]. Characteristics of these 14 seamounts were compared with measurements from Seasat altimeter profiles.

From the 14 detailed maps we extracted several basic characteristics of each seamount (Table 1). Their positions were determined from the highest point on the seamount or the center of the flat-topped summit of the guyot. The height of the seamount, from base to summit, and three characteristic seamount contours were measured. The summit diameter of each guyot was determined from the circle about the center of the seamount that best matches the contour of the slope break. Two other characteristic diameters were also measured

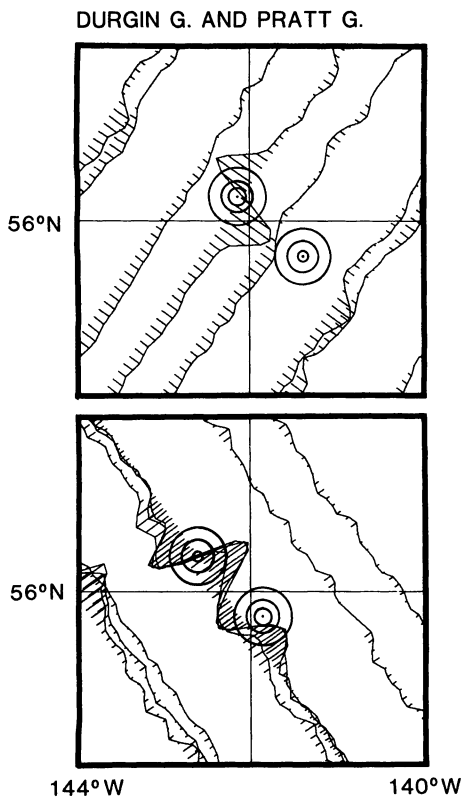

Fig. 4. Along-track vertical deflection profiles over Durgin Guyot and Pratt Guyot [Sandwell, 1984*b*]. The three circles are idealized contours at the seamount's base, half way to the summit, and the summit. The seamount is located along a line perpendicular to the profile at the zero crossing of the vertical deflection profile. The peak and trough line up with the second circle (i.e., the half diameter). These seamounts formed on relatively young lithosphere (~15 Ma) and have small flexural diameters.

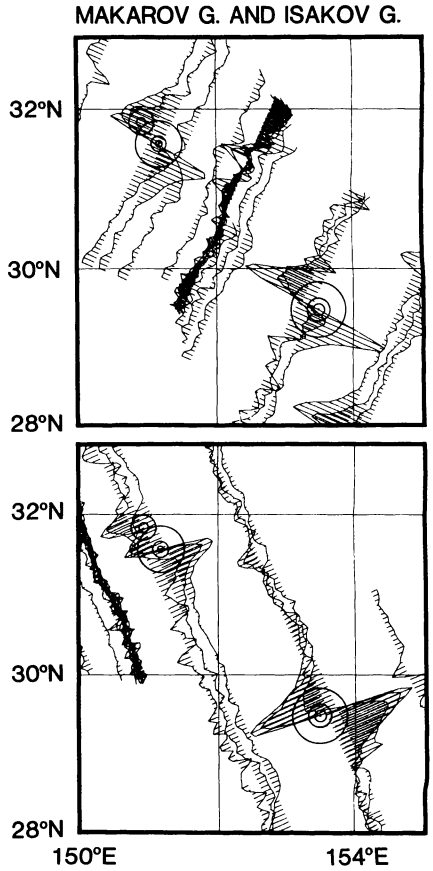

Fig. 5. Vertical deflection profiles over Makarov Guyot and Isakov Guyot The peak and trough of each profile line up with the second circle (i.e., the half diameter). These seamounts formed on relatively old lithosphere (~50 Ma) and have large flexural diameters.

using this method; they are the diameter of the base of the seamount and the diameter of the seamount half way between the base and the summit. When the seamount had more than one summit (e.g., Ojin Guyot), the measurements were made using only the summit nearest the satellite profile; the adjacent volcanic cones were ignored. These basic contours do not contain any information about the ellipticity or complex shape of the seamount. Such detailed information is not usually recoverable, however, because of upward continuation of the gravitational potential through the water column.

Along-track vertical deflection profiles over four guyots are shown in Figures 4 (Durgin Guyot and Pratt Guyot) and 5 (Makarov Guyot and Isakov Guyot). The three circles represent the three basic contours of the guyot. Both the ascending (bottom) and descending (top) vertical deflection profiles show the characteristic peak-and-trough signature of a seamount. The spacing between data points (vertical lines) is 6.6 km, and the vertical scale is 60 μrad per degree of longitude. In all cases, the center of the seamount is located along the line, perpendicular to the profile, that passes half way between the peak and the trough. The along-track location can be measured to an accuracy of 5 to 10 km. The amplitude of the vertical deflection signature depends on the minimum distance between the profile and the center of the seamount (y_c) as predicted by the model.

The model also predicts that the half diameter of the seamount is equal to the distance between the peak and the trough of the along-track vertical deflection profile. Although it is difficult to see in these figures, the distance between the peak and trough is equal to or slightly greater than the diameter of the second circle (i.e., the half diameter). Moreover, the peak-to-trough distance does not depend strongly on y_c. To determine the accuracy of the agreement, peak-to-trough distances for all profiles intersecting the 14 seamounts were measured (Table 1) and compared with the actual half diameter. A plot of the peak-to-trough diameter versus the half diameter is shown in Figure 6. The octagons are peak-to-trough distances for the profile that passes closest to the center of each seamount (measurement 1 in Table 1). The triangles are distances made from other profiles that pass over the seamount. If the agreement were perfect, the points would lie on the dashed line. In fact, the scatter about this line is about 10 km except in the case of the smallest seamounts, where the disagreement is greater and systematic. The problem in measuring the diameters of the smallest seamounts is due to the noise in the altimeter data and the low-pass filter (cutoff wavelength of 21 km) used to suppress the noise. Measurements will improve when more accurate satellite altimeter data (e.g., Geosat) are available. These initial results suggest that a single satellite altimeter profile can be used measure seamounts with diameters greater than 30 km to an accuracy of 10 km.

A third model prediction is that the flexural rigidity of the lithosphere when the seamount formed can be estimated from a single satellite altimeter profile. According to the model the flexural diameter is equal to the deflection diameter (zero crossing to zero crossing) minus the seamount diameter (peak-to-trough). To test the model, we measured the deflection diameter of the satellite altimeter profile that passed closest to the center of each seamount and

TABLE 1. Seamount Measurements

Seamount	Latitude, deg	Longitude, deg	Height, m	Summit Diameter, km	Half Diameter, km	Basal Diameter, km	Peak-to-Trough Diameter, km 1	2	3	4
Durgin G.	55.84	-141.86	2745	12.5	23.4	41.8	26.4	29.7	29.7	33.0
Pratt G.	56.23	-142.62	2726	07.2	22.6	40.4	25.1	27.8	23.1	29.7
Ojin G.	37.98	170.37	4758	23.0	54.6	94.8	58.1	51.5	52.8	-
Jingu G.	38.66	171.15	4941	20.0	43.2	77.6	38.3	39.0	39.6	38.3
Makarov G.	29.48	153.49	4063	16.4	33.0	75.4	29.7	31.7	33.0	36.3
Isakov G.	31.57	151.17	4209	08.6	21.4	64.2	25.1	26.4	29.7	31.7
Magnet S.	12.23	173.20	4000	-	14.8	39.4	22.5	31.7	-	-
H11 S.	26.45	-177.86	4100	-	16.8	35.8	27.7	-	-	-
Uyeda S.	-7.55	-151.53	3500	-	33.0	65.8	34.4	29.7	-	-
Mahler S.	31.93	-164.95	3000	-	17.4	30.8	26.4	-	-	-
Schubert S.	31.90	-163.13	2500	06.4	22.6	43.4	27.7	-	-	-
Debussy S.	30.40	-162.06	3500	-	33.6	48.4	35.0	-	-	-
Tchaikovski S.	29.40	-162.12	3500	-	12.0	22.8	19.8	-	-	-
Heezen G.	8.81	163.20	4000	12.6	31.6	76.0	31.7	42.9	52.8	62.8

G., guyot; S., seamount

computed the flexural diameter (Table 2). Measurements of the deflection diameter are only accurate to about 20 km because of the sensitivity of the zero crossing to noise. Estimates of the age (and age uncertainty) of the lithosphere when each seamount formed were found in the literature for 12 of the 14 seamounts [*Smoot*, 1981; *Clague and Dalrymple*, 1975; *Jackson et al.*, 1980; *Sager*, 1983; *Vogt and Smoot*, 1984]. In general, the age estimates are very uncertain since they depend on both plate tectonic models [*Larson et al.*, 1985] for the seafloor age and rock samples for radio isotope or fossil age estimates (Table 2).

The observed flexural diameter versus loading age was compared with the prediction of the model (Figure 7). Most of the seamounts (e.g., Durgin Seamount, Pratt Seamount and Musician Seamounts) formed on lithosphere with an age less than 20 Ma and have smaller flexural diameters (<80 km). Makarov Guyot and Isakov Guyot both formed on older lithosphere (>35 Ma) and have larger flexural diameters (>140 km). These are first-order differences that are evident in the data (see Figures 4 and 5) and and roughly agree with the model. The data from Ojin Guyot and Jingu Guyot do not agree with the model and are not shown in Figure 7. We believe the disagreement occurs because the model assumes that the volcanoes are isolated whereas in this case there are three large volcanic loads within one flexural radius of each other. *Watts and Ribe* [1984] have constructed a more detailed and accurate model of these clustered volcanoes and find good agreement with the Seasat altimeter data. They also noted that the overall diameter of the geoid signature is diagnostic of the strength of the lithosphere when the seamount formed.

Overall, these findings suggest that the flexural diameter of the lithosphere when the seamount formed can be measured from a single satellite altimeter profile when conditions are favorable. First, the seamount must be isolated and have only one major peak. Second, the amplitude of the vertical deflection signature must be at least 5 times larger than the noise level of the altimeter profile. Finally, a more quantitative method of measuring the zero-crossing points is needed. It should be noted that these conditions are rarely met with the currently available data from Seasat.

GLOBAL ANALYSIS

Signals corresponding to seamounts were identified by eye, treating the ascending and descending tracks independently. Each seamount was located at the central zero crossing on the track with the highest-amplitude signal. The actual location of the seamount's summit is along a line perpendicular to the track at the zero crossing. The following criteria were adopted to identify a seamount: (1) the signal must have a positive and a negative lobe (peak and trough), (2) the peak and trough must be of comparable amplitudes, (3) there must be three zero crossings, (4) there must be at least two data points in each lobe, (5) it must not be possible to trace the signal on more than three widely spaced tracks (~150 km apart), (6) areas of seafloor shallower than 1000 m were excluded, and (7) one seamount from any pair with digitized locations less than 15 km apart was discarded.

Criteria 1, 2, and 3 are based on the shape of the seamount signal modeled in previous sections (Figure 2). Criterion 4 is a crude low-pass filter, removing signals less than about 15 km wide. Criterion 5 defines the attempt made to counter the most pervasive systematic error: the difficulty of separating seamount signals from those associated with linear features such as fracture zones and ridges. In many cases, where repeat tracks lie close together, it is possible to see a signal from the same seamount on more than one track, and those cases will be important for detailed two-dimensional modeling of the seamounts. But since the extent of any isolated seamount's signal, measured along-track, is rarely more than 100 km (and the peak-to-trough distance is much less than that), a signal which spreads across

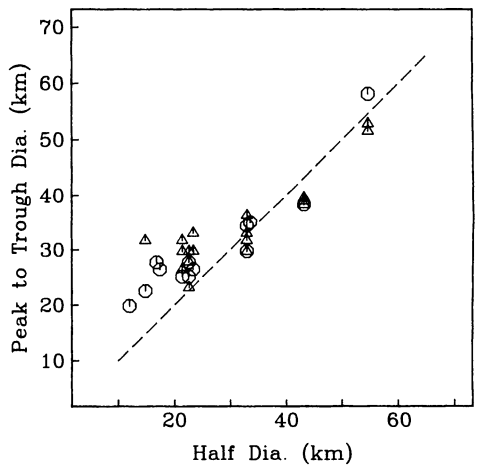

Fig. 6. Peak-to-trough diameters from vertical deflection profiles over 14 seamounts versus the half diameter of the seamount. Octagons represent profiles that passed close to the center of the seamount. Triangles represent profiles that pass away from the seamount's center.

TABLE 2. Seamount Diameters

Seamount	Seafloor Age, Ma	Seamount Age, Ma	Loading Age, Ma	Deflection Diameter, km	Flexural Diameter, km
Durgin G.	26	12	14±4	92.4	66.0
Pratt G.	32	13	19±4	85.8	60.7
Ojin G.	110	66	44±10	224.4	166.3
Jingu G.	110	66	44±10	211.2	172.9
Makarov G.	156	94	62±4	178.2	148.5
Isakov G.	141	102	39±4	171.6	146.5
Magnet S.	140	-	-	99.0	76.5
H11 S.	118	>74	<44	105.6	77.9
Uyeda S.	85	68-72	15±2	108.9	74.5
Mahler S.	100	85-95	10±7	56.1	29.7
Schubert S.	97	85-95	8±7	92.4	64.7
Debussy S.	95	85-95	7±7	95.7	60.7
Tchaikovski S.	93	85-95	8±7	52.8	33.0
Heezen G.	170	-	-	132.0	100.3

G., guyot; S., seamount

several tracks must relate to a topographic feature that is elongated in the same direction. Criterion 5 also eliminates small swells or plateaus. To ensure self-consistency and to avoid making unnecessary judgements about the quality of bathymetric data all topographic features on the seafloor were identified from their signals in the deflection of the vertical. Adoption of criterion 6 ensures that all the seamounts are located on oceanic crust. Criterion 7 is applied to remove some of the duplication between seamounts identified on both ascending and descending tracks; criterion 4 has already established that seamounts smaller than 15 km will not be resolved. Seamounts with broader signals that are crossed by both sets of tracks remain counted twice; we will use a mass dipole model to distinguish between a single broad signal and two close small ones in future work.

Despite the obvious subjectiveness of this method, the results are more reliable than the only current feasible alternative: the matched filter technique [e.g., *Lazarewicz and Schwank,* 1982]. The latter method uses individual profiles without regard to the signals on adjacent profiles. In many cases, vertical deflection profiles over fracture zones have the characteristics of seamount signatures. In these cases the matched filter technique will misidentify this fracture zone as a chain of seamounts.

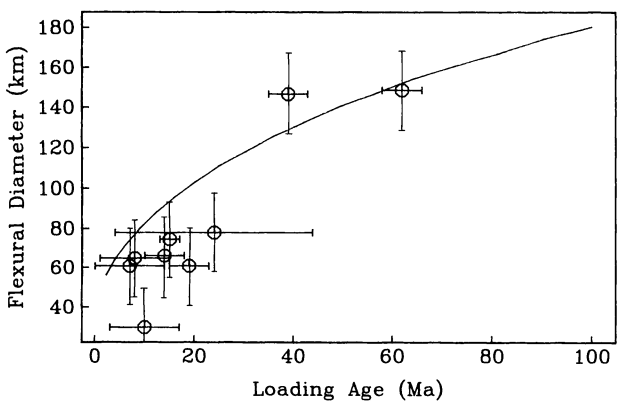

Fig. 7. Flexural diameter versus the age of the lithosphere when the seamount formed (solid curve). The flexural diameter is equal to the deflection diameter minus the seamount diameter (see Fig. 3). Measurements of flexural diameter from vertical deflection profiles over nine seamounts (octagons). Many of the loading age estimates are uncertain.

After locating the seamounts, two characteristic dimensions of each seamount's vertical deflection signal were measured: the distance between the peak and trough and the peak-to-trough amplitude. The peak and trough were located by a program capable of searching all the Seasat data within an assigned radius of the seamount's location. The values and location of the maximum and minimum within the specified region were used to calculate and store the amplitude and width for each seamount.

Computed results were compared with handmade measurements in the northeast Pacific (GEBCO sheet 7; 0° to 47°N, 90° to 180°W), which contains seamounts with a wide range of sizes. The choice of search radius for the computer program was constrained by the need to make the radius large enough not to exclude the peaks and trough

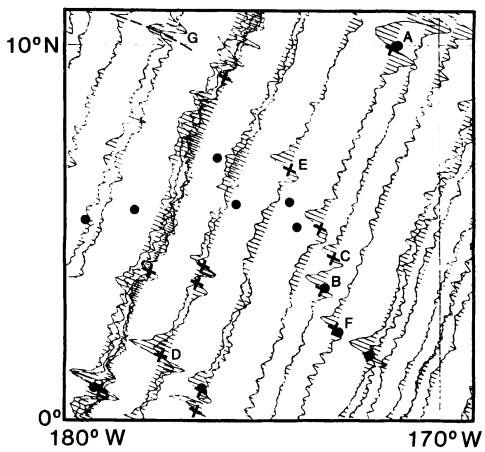

Fig. 8. Values of the deflection of the vertical plotted perpendicular to descending Seasat tracks (scale = 60 μrad/deg of longitude). Each stroke represents one data point. Seamount locations are marked by crosses. The circles represent picks made from the deflection of the vertical along the ascending tracks. A and B are examples of signatures fulfilling all criteria 1–6. C and D are examples of signatures where one zero crossing is lost in the noise. E and F are examples of signatures which are very asymmetric. G is part of a linear feature. Out of the 26 separate locations in this region, six are probably duplicated on the two sets of tracks. Comparing the Seasat data with the GEBCO bathymetric chart: ten picks are close to charted seamounts; five picks lie in areas with no bathymetric data; two picks lie on irregularities in the Magellan Rise; three picks are not near to charted seamounts, even though ship tracks go close to them; and two charted seamounts, which lie between satellite tracks, are not visible in the satellite data.

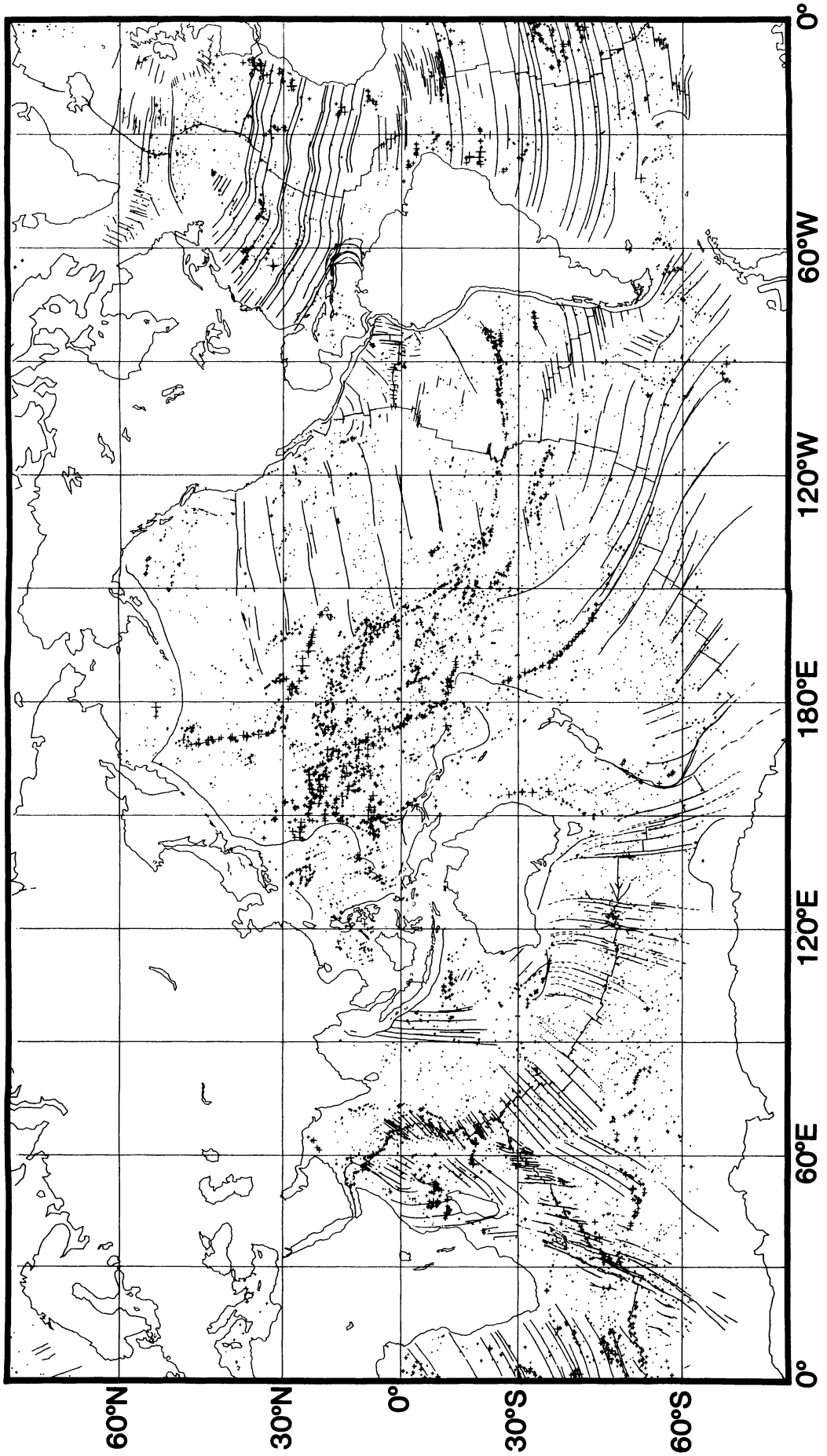

Fig. 9. Global map showing the location of all seamounts identified in the Seasat data with signatures in the deflection of the vertical that have peak-to-trough amplitudes greater than 15 μrad; symbol size is proportional to signal amplitude.

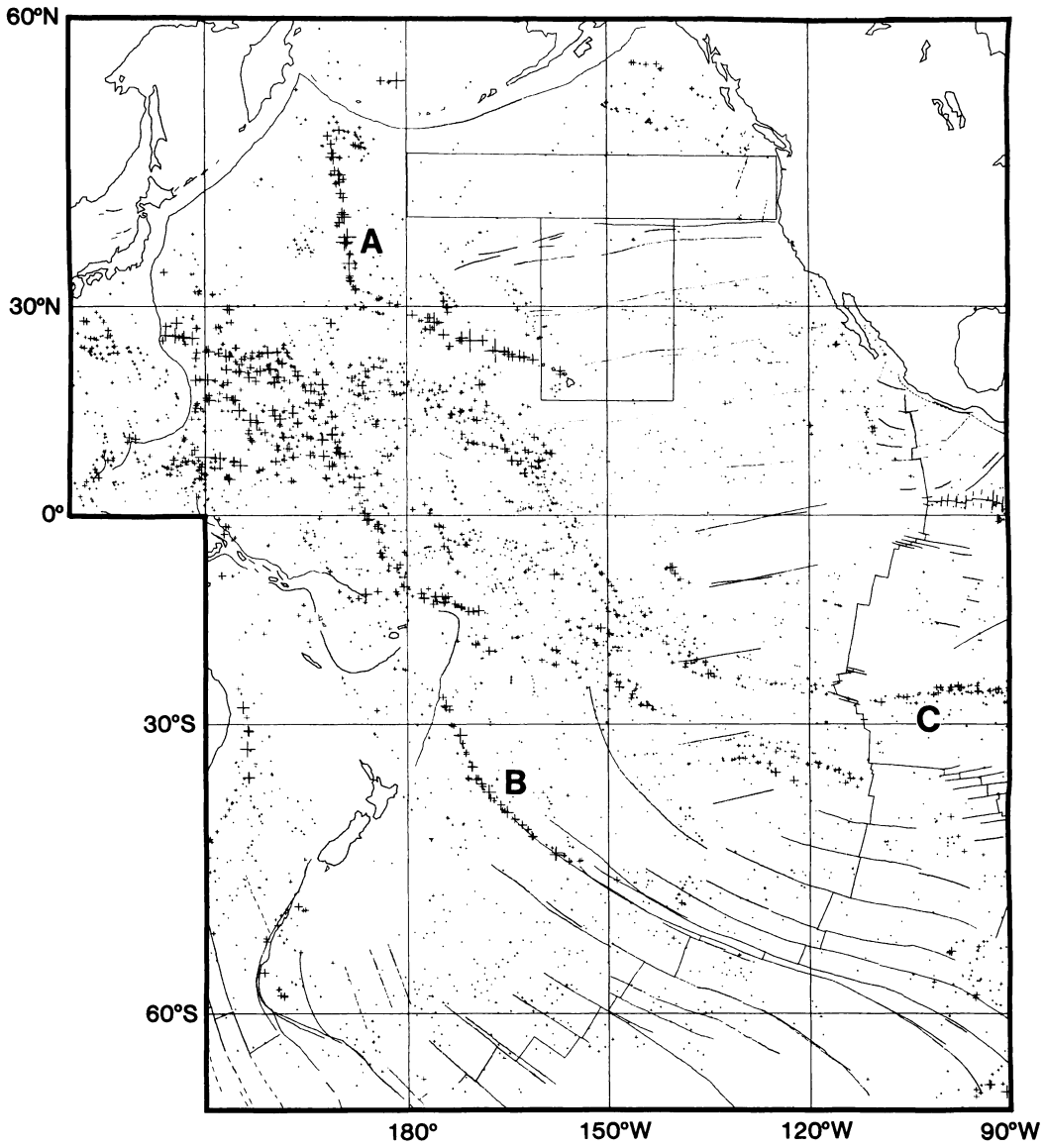

Fig. 10. Seamounts in the Pacific Ocean; symbol size is proportional to signal amplitude, and signals smaller than 15 μrad are excluded. Labeled features are A, the Hawaiian-Emperor seamount chain; B, the Louisville Ridge; C, the Sala y Gomez Ridge.

of a large seamount, and therefore underestimate its amplitude and width, and the need to keep it small enough not to overestimate the size of small seamount by including higher-amplitude signals off to the sides. In fact, even the largest seamounts typically have only two data points between the central zero crossing and a maxima, corresponding to about 13 km half radius. Comparing the handmade measurements with values computed using a search radius of 30 km showed close agreement (better in width than amplitude, which is difficult to measure accurately by hand) in all but a very few cases.

RESULTS

A total of 8556 seamount locations have been identified: 4887 on descending tracks and 3669 on ascending ones. The greatest difference in numbers between the two sets of tracks occurs in the Indian Ocean, where there are many fracture zones that run subparallel to the descending tracks. The fracture zone signals are easy to pick out on the ascending tracks, which cross them at high angles but may have interfered with the identification of seamounts on the descending tracks. Although most seamounts are only picked out once, there is duplication between the two sets of locations (see Figure 8), and detailed modeling will be necessary to find duplicates. Assuming seamounts are not organized along satellite tracks, this ambiguity affects the absolute number of seamounts located but not the relative population densities in different areas. The complete set of locations is shown in Figure 9; the Pacific, Atlantic, and Indian oceans are plotted separately in Figures 10–12, respectively. In all plots the seamounts with amplitudes less than 15 μrad have been excluded, and the symbols are scaled by the amplitude of the signal. Some of the features that we describe can be detected in bathymetric charts, but they are more easily identified in Seasat data.

As is well-known, the seamount population density is higher in the west Pacific than in the east [*Menard*, 1964]. The density increases west of about 200°E and is highest between 25°N and 20°S. Our maps (Figures 9 and 10) show that within the high-density area, which has many large seamounts, there are several lineations subparallel to the

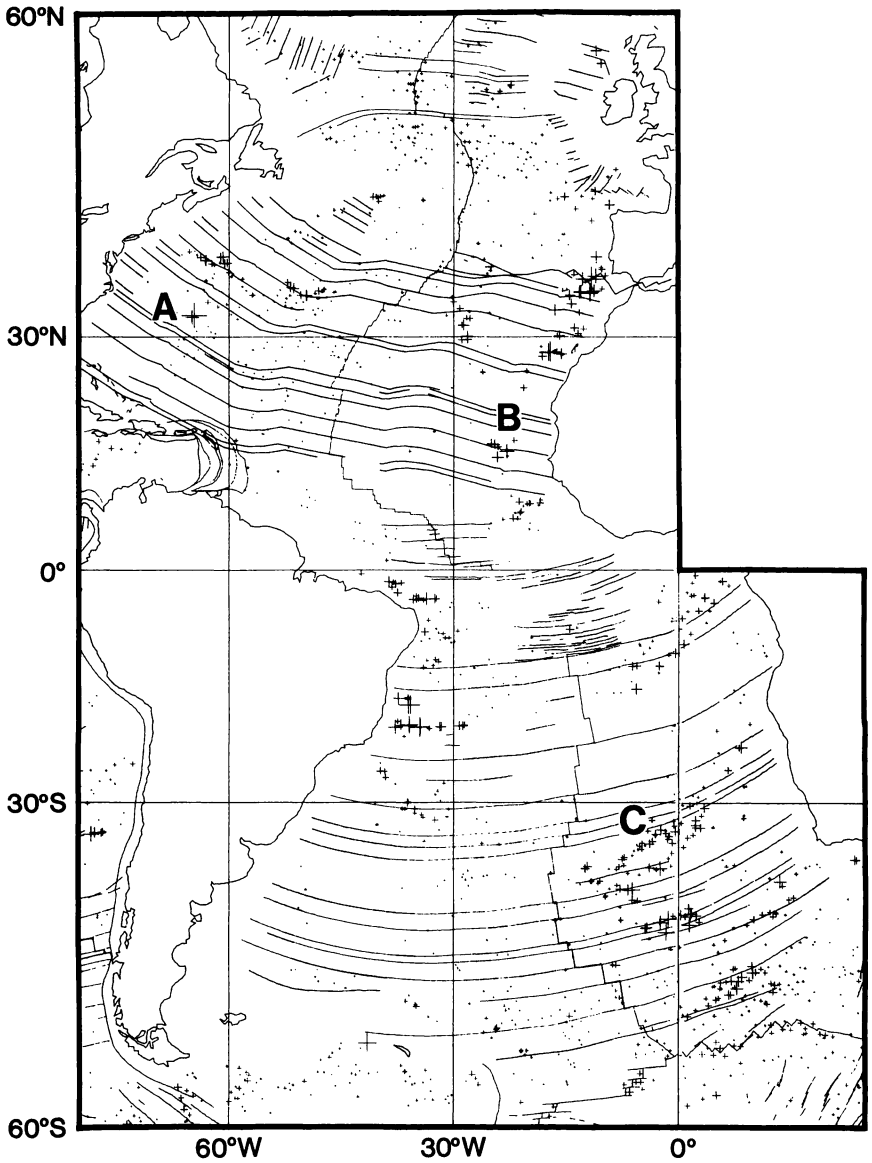

Fig. 11. Seamounts in the Atlantic Ocean; symbol size is proportional to signal amplitude, and signals smaller than 15 μrad are excluded. Labeled features are A, the Bermuda Rise; B, the Cape Verde Islands; C, the Walvis Ridge.

Hawaiian-Emperor trends. Seamount chains include the Mariana, Gilbert, Tuomotu, and Austral island groups, with several possible smaller chains beside them between 150°E and 150°W. There are no large-amplitude seamounts in the northeast Pacific (Figure 10), and two areas that are almost devoid of seamounts stand out; one is a strip of seafloor, 20° wide, running north-south along the line of longitude 210°E and the other lies north of the Mendocino fracture zone. The pattern of seamounts in the South Pacific was previously very poorly mapped. It is dominated by the Louisville and Sala y Gomez ridges and the southern part of the high-density western region, which extends no farther than about 20°S. All the seamounts south of the southern end of the Louisville Ridge are medium sized or small in amplitude.

The high-amplitude seamounts in the Atlantic occur in tight clusters (Figure 11); usually in a region where there is some other evidence of hotspot activity (such as the Walvis Ridge, Bermuda, Cape Verde Islands, etc.). Unlike in the Atlantic, the seamount distribution in the Indian Ocean and south of Australia is uniform. There is little variation in size within the Indian Ocean (Figure 12) except over the large seamounts of the Cosmoledo Group north of Madagascar and two other smaller clusters (Figure 12). The northeast-southwest trending fracture zones probably interfere with the seamount signals in the north Indian Ocean where the population density is slightly higher and the fracture zones are more closely spaced than in surrounding areas. The seamount distribution appears to vary little between 90°E and 150°E and shows no change over the Australian-Antarctic Discordance; there is no interference from fracture zone signals on the ocean floor south of Australia, where the fracture zones run approximately north-south and are cut at high angles by both sets of Seasat tracks.

Our results suggest that the age differences associated with fracture zones may influence the distribution of seamounts. In the east Pacific (Figure 13) the population density is invariably higher on the younger side of each large age-offset fracture zone, from the Mendocino to the Marquesas, creating strips of seafloor with different densities. The ocean floor between the Galapagos and Marquesas

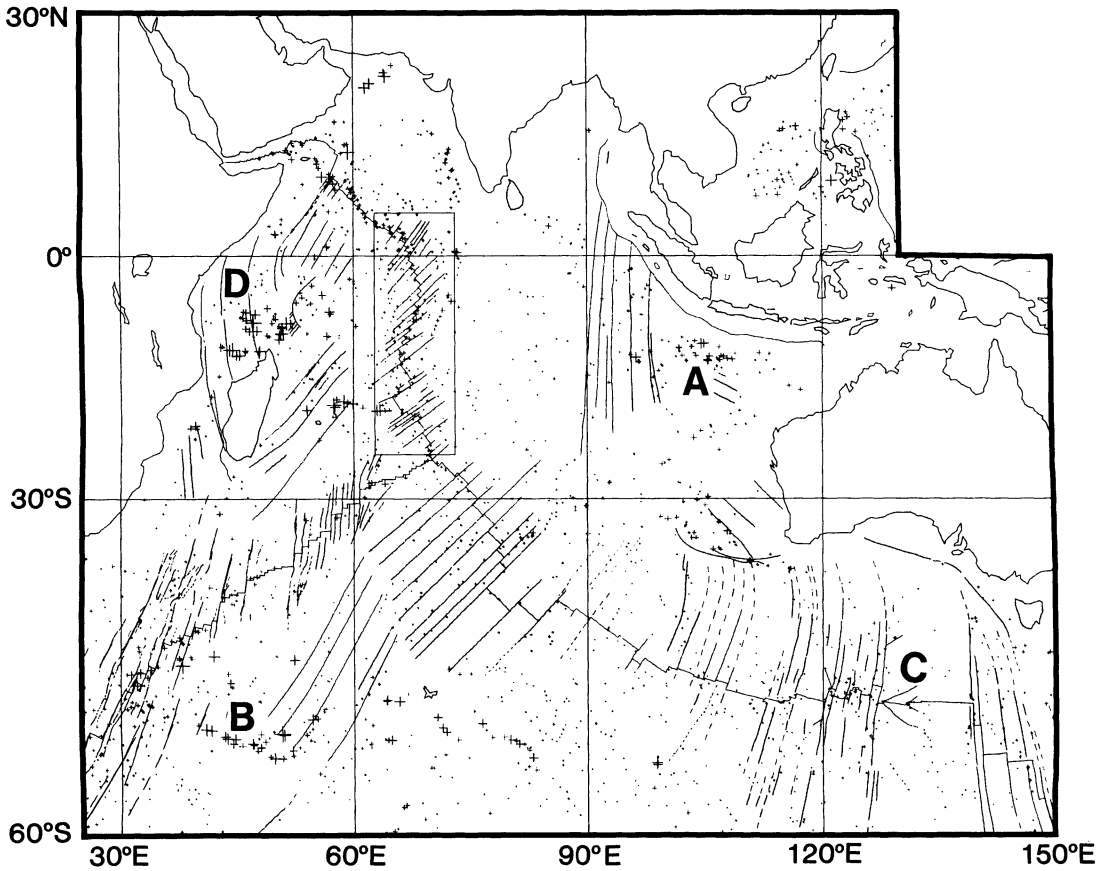

Fig. 12. Seamounts in the Indian Ocean; symbol size is proportional to signal amplitude and signals smaller than 15 μrad are excluded. Labeled features are A, Vening-Meinesz seamounts; B, Crozet Island and Conrad Rise; C, the Australian-Antarctic Discordance; D, the Cosmoledo seamount group.

fracture zones, which is older than that to its north and south, has the lowest density of seamounts.

The measured widths of seamounts vary from about 14 to 55 km and do not show clear spatial variations between oceans. A histogram of the width-frequency distribution, for all the located seamounts (Figure 14), peaks in the range 23–30 km. Without detailed modeling of each signature the current width resolution is limited by the data point spacing of 6.6 km. No widths greater than 60 km (the diameter of the search area) were measured, but the frequency is clearly close to zero above the 51–58 km bin. Most of the seamounts sampled have a peak-trough width of four data point intervals (26.4 km) and the number of seamounts decreases with increasing diameter in agreement with previous studies [*Jordan et al.*, 1983: *Smith and Jordan*, 1988]. The number of seamounts also decreases with decreasing diameter (stippled area in Figure 14). This decrease is an artifact due to poor resolution. The signals from narrow seamounts, which are low because of the small volume of the seamounts, are further damped by the low-pass filter applied to the Seasat profiles (cutoff wavelength of 21 km) as well as by upward continuation through the seawater. Therefore our location and measurement technique vastly underestimates the numbers of small seamounts.

The amplitude-frequency histogram of all the seamounts (Figure 15) is smooth on the scale of ~1 μrad and sharply peaked at 15–25 μrad, falling off rapidly below 15 μrad and more gradually between 20 and 100 μrad. A long tail in the distribution extends from 100 to just below 400 μrad. The decrease in number with increasing amplitude is partly due to the decrease in the number of large seamounts and partly due to the fact that Seasat profiles do not usually intersect the crest of each seamount. The rapid decrease in frequency for amplitudes less than 15 μrad (stippled area in Figure 15) is an artifact due to the limited accuracy of Seasat data (~7 μrad). There are 1012 of these smaller-amplitude seamount signatures that were not included in the seamount maps (Figures 9–13). Eliminating all seamounts with signals below 15 μrad has little effect on the southern oceans but makes the Hawaiian-Emperor chain stand out more clearly from the background distribution in the North Pacific.

The range in amplitudes is much larger than that in widths because several additional factors affect the amplitude of the observed signal. The width of the vertical deflection signature is primarily a measure of the width (or volume) of the seamount. In contrast, the amplitude of the geoid signature depends on seamount volume, the degree of compensation experienced by the seamount, and the distance between the summit of the seamount and the satellite pass. Both increasing compensation and increasing distance from the seamount summit to the satellite profile reduce the amplitude of the geoid signature. Since the degree of compensation is a function of the age of the oceanic crust at the time of volcanic loading, it does not have straightforward spatial variations (i.e., ocean floor of the same age can have on it seamounts with different degrees of compensation).

Watts and Ribe [1984] conclude that because of these problems, it may not be possible to use satellite altimetry to predict bathymetry in the oceans with any degree of reliability. Despite these difficulties, our results indicate that several basic characteristics of seamounts can be measured from single satellite altimeter profiles. In future

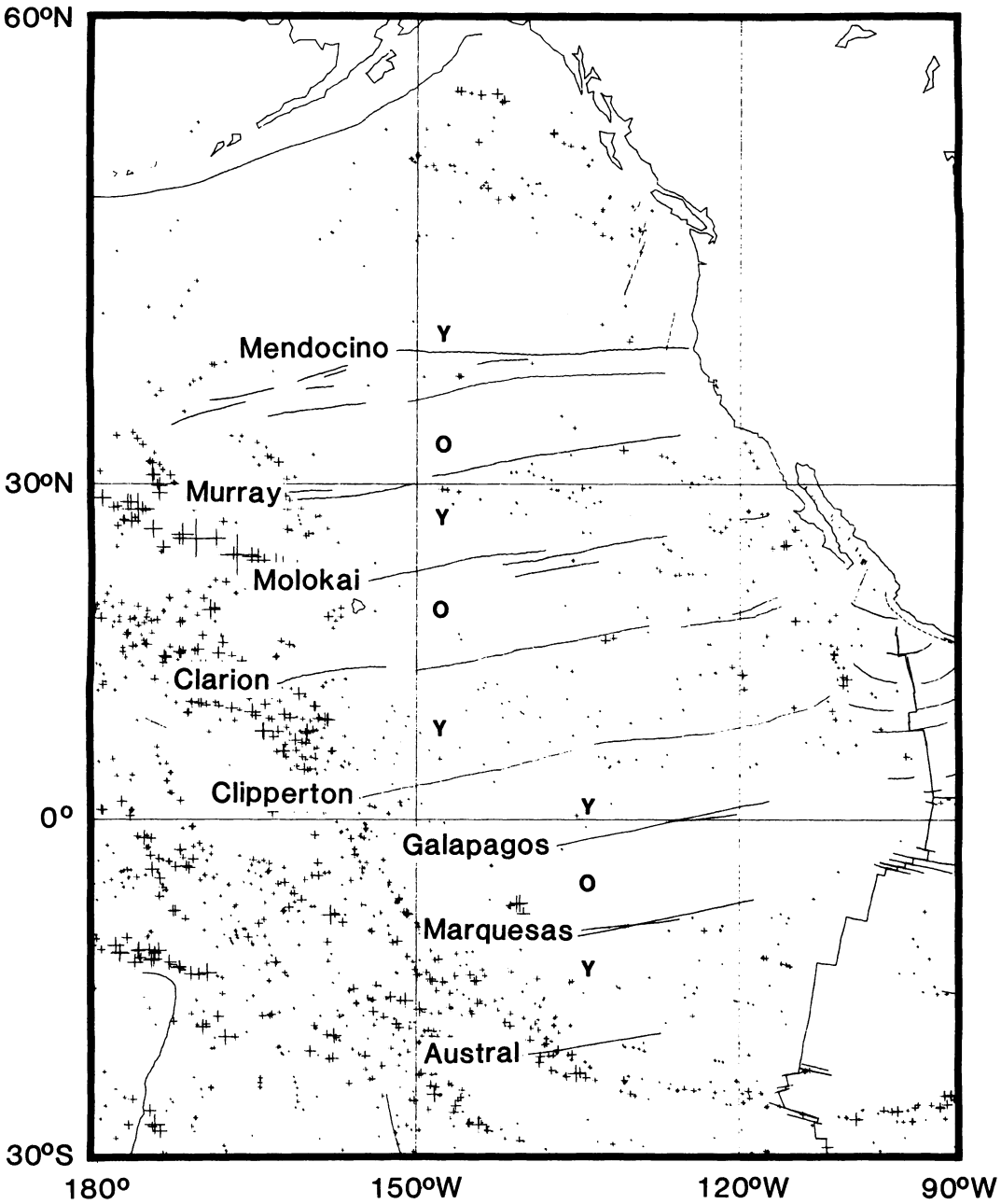

Fig. 13. Seamounts in the NE Pacific; symbol size is proportional to signal amplitude, and signals smaller than 15 μrad are excluded. The younger (Y) and older (O) seafloor on either side of each of the large age-offset fracture zones is labeled. The seamount population density decreases from the young to old sides of most fracture zones.

work we hope to do two-dimensional fits to seamounts that have clear signals and estimate the off-track location and maximum amplitudes of the signal.

CONCLUSIONS

The basic characteristics of a seamount that can be measured from a single satellite altimeter profile are as follows:

1. The along-track location of the center of the seamount can be determined to an accuracy of less than 10 km. The accuracy of the cross-track location is limited by the data distribution [*Baudry et al.*, 1987].

2. The characteristic diameter of a seamount is equal to the distance between the peak and the trough of the vertical deflection signature. This measurement is accurate to about 10 km as long as the profile passes somewhere over the bathymetric expression of the seamount. The accuracy degrades as the width of the seamount approaches the resolution of the altimeter profile.

3. The flexural diameter of a seamount is related to the age of the lithosphere when the seamount formed. As long as the seamount is isolated, the flexural diameter is equal to the overall diameter of the vertical deflection signature (zero crossing to zero crossing) minus the peak-to-trough diameter. At best, the flexural diameter can be measured to an accuracy of 20 km, although this accuracy degrades

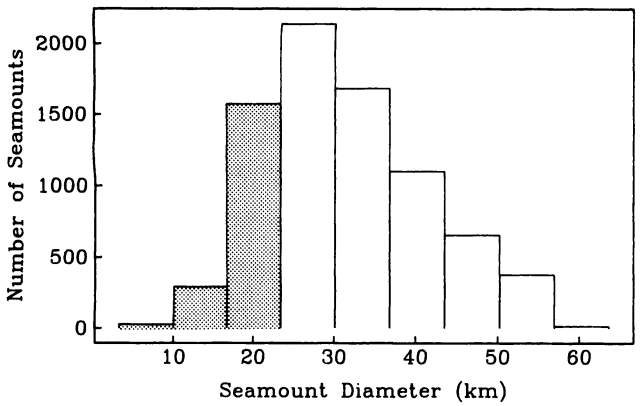

Fig. 14. Histogram of the diameter (peak-to-trough separation) of all the seamounts identified in the Seasat data (bin width = 7 km).

as the ratio of the signature amplitude to altimeter noise decreases.

Seamount distributions derived from satellite altimetry provide a useful basis for comparisons between different regions because the sampling is uniform in density and quality. It is straightforward to obtain measurements of the width of every located seamount and the amplitude of its gravitational signal. From the global analysis of the Seasat profile data the following points emerge:

1. Large-scale differences in population density, which are not always visible in bathymetric charts, are shown clearly here: the density is higher in the western than eastern Pacific and higher in the west Pacific than the Atlantic or Indian oceans.

2. Seamounts with large-amplitude signals are in the high-density Pacific region or in clusters in the Atlantic.

3. The west Pacific shows several lineations in its seamount distribution, subparallel to the Hawaiian-Emperor chain.

4. The South Pacific, which has poor bathymetric mapping, has low but fairly uniform numbers of seamounts.

5. The density of seamounts in the east Pacific is higher on the younger side of every large age-offset fracture zone.

6. The Indian Ocean contains mainly small- to medium-sized seamounts.

7. The number of seamounts smoothly decreases with amplitude between 20 and 100 μrad and decreases with width above 23 km. Below these values the numbers in both types of distribution are reduced by the problems of identifying seamount signals in the deflection of the vertical, some of which would be removed by improved data or data coverage.

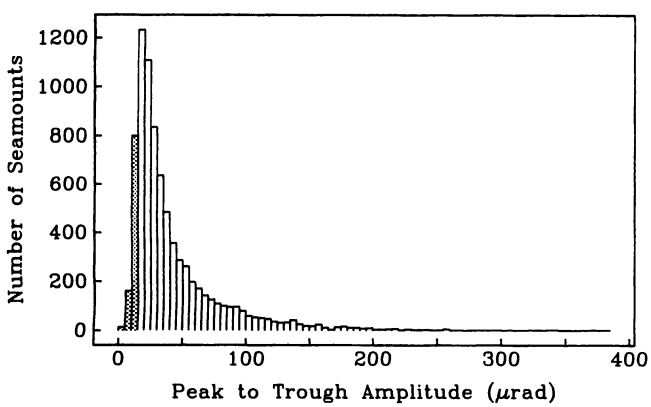

Fig. 15. Histogram of the amplitudes of all the seamount signals identified in the Seasat data (bin width = 5 μrad).

The accuracy of the measurements will improve as the accuracy and coverage of satellite altimeter data improves. The Geosat mission [*Cheney et al.*, 1986] demonstrates that altimeter accuracies can be improved by a factor of 4 over the Seasat accuracy. This improves the along-track resolution by nearly a factor of 2. Moreover, Geosat coverage (from the classified geodetic mission) is more than 10 times better than Seasat coverage. This level of coverage may become available with the ERS 1 satellite planned by the European Space Agency. Simple measurements of satellite altimeter profiles will provide important information on the distribution, sizes, and ages of seamounts in the oceans. These data will place tight constraints on the processes that control the birth and development of undersea volcanoes.

Acknowledgments. We thank Rodey Batiza, Rick Blakely, and Ross Stein for their critical and helpful reviews of the original manuscript. This work was supported by the NASA Geodynamics Program (NAG 5-787).

REFERENCES

Banks, R.J., R.L. Parker, and S.P. Heustis, Isostatic compensation on a continental scale: Local versus regional mechanisms, *Geophys. J. R. Astron. Soc., 51*, 431–452, 1977.

Batiza, R., Lithospheric age dependence of off-ridge volcano production in the North Pacific, *Geophys. Res. Lett., 8*, 853–856, 1981.

Baudry, N., and M. Diament, Confirmation with ship data of Seasat bathymetric predictions in the south central Pacific, *Geophys. J. R. Astron. Sci.*, in press, 1988.

Baudry, N., M. Diament and Y. Albouy, Precise location of unsurveyed seamounts in the Austral archipelago area using Seasat data, *Geophys. J. R. Astron. Sci., 89*, 869–888, 1987.

Bracewell, R.N., *The Fourier Transform and Its Application*, McGraw-Hill, New York, 1978.

Canadian Hydrographic Service, General bathymetric chart of the oceans (GEBCO), 5th ed., Ottawa, Ont., Canada, 1982.

Cheney, R., B. Douglas, R. Agreen, L. Miller, D. Milbert, and D. Porter, The Geosat altimeter mission: A milestone in satellite oceanography, *Eos Trans. AGU, 657*, 1354–1356, 1986.

Claque, D.A., and G.B. Dalrymple, Cretaceous K-Ar ages of volcanic rocks from the Musician Seamounts and the Hawaiian Ridge, *Geophys. Res. Lett., 2*, 305–308, 1975.

Gass, I.G., D.S. Chapman, H.N. Pollack, and R.S. Thorpe, Geological and geophysical parameters of mid-plate volcanism. *Philos.Trans. R. Soc. London, Ser. A, 288*, 581–597, 1978.

Jackson, E.D., et al., Introduction and summary of results form DSDP leg 55, the Hawaiian-Emperor hot-spot experiment, *Initial. Rep. Deep Sea Drill. Proj., 55*, 5–31, 1980.

Jordan, T.H., H.W. Menard, and D.K. Smith, Density and size distribution of seamounts in the eastern Pacific inferred from wide-beam sounding data, *J. Geophys. Res., 88*, 10,508–10,518, 1983.

Lambeck, K., and R. Coleman, A search for seamounts in the southern Cook and Austral region, *Geophys. Res. Lett., 9*, 389–392, 1982.

Larson, R.L., W.C. Pitman, X. Goloychaiko, S.C. Cande, J.F. Dewey, W.F. Haxby, and J. L. LaBrecque, The bedrock geology of the world, map, W.H. Freeman, New York, 1985.

Lazarewicz, A.R., and D.C. Schwank, Detection of uncharted seamounts using satellite altimetry, *Geophys. Res. Lett., 9*, 385–388, 1982.

Marsh, J. G., and T. V. Martin, The Seasat altimeter mean sea surface model, *J. Geophys. Res., 87*, 3269–3280, 1982.

Menard, H.W., *Marine Geology of the Pacific*, McGraw-Hill, New York, 1964.

Sager, W.W., Seamount paleomagnetism and Pacific plate tectonics, Ph.D. thesis, Univ. of Hawaii at Manoa, Honolulu, 1983.

Sandwell, D.T., A detailed view of the South Pacific geoid from satellite altimetry, *J. Geophys. Res., 89*, 1089–1104, 1984*a*.

Sandwell, D.T., Along-track deflection of the vertical from Seasat: GEBCO overlays, *NOAA Tech. Memo., NOS NGS-40*, 1984*b*.

Sandwell, D.T. and G. Schubert, Lithospheric flexure at fracture zones, *J. Geophys. Res., 87*, 4657-4667, 1982.

Smith, D.K. and T.H. Jordan, Seamount statistics in the Pacific Ocean, *J. Geophys. Res., 93*, 2899–2918, 1988.

Smoot, N.C., Multi-beam sonar surveys of guyots of the Gulf of Alaska, *Mar. Geol., 43,* M87–M98, 1981.

Smoot, N.C., Guyots of the Mid-Emperor Chain mapped with multi-beam sonar, *Mar. Geol., 47,* 153–163, 1982.

Smoot, N.C., Multi-beam surveys of the Michelson Ridge guyots: Subduction or obduction, *Tectonophysics, 99,* 363–380, 1983.

Spence, D.A., and D.L. Turcotte, Magma-driven propagating cracks, J. *Geophys. Res., 90,* 575–580, 1985.

Vogt, P.R., Volcano height and plate thickness, *Earth Planet. Sci. Lett., 23,* 337–348, 1974.

Vogt, P.R., and N.C. Smoot, The Geisha Guyots: Multibeam bathymetry and morphometric interpretations, *J. Geophys. Res., 89,* 11,085–11,107, 1984.

Watts, A.B., and N.M. Ribe, On geoid heights and flexure of the lithosphere, *J. Geophys. Res., 89,* 11,152–11,170, 1984.

C. H. Craig, Home Office, Abell House, John Islip Street, London, SW1P 4LH, England.

D. T. Sandwell, Center for Space Research, University of Texas at Austin, Austin, TX 78759.

(Received April 13, 1987;
Revised December 23, 1987
accepted October 26, 1987.)